Chemical Physics Letters 782 (2021) 139028

Contents lists available at ScienceDirect

Chemical Physics Letters

journal homepage: www.elsevier.com/locate/cplett

Research paper

Spectral transition properties of the $A^1\Pi$-$X^1\Sigma^+$ system for PN

Zhi Qin [a,b], Tianrui Bai [a,c], Linhua Liu [a,c,d,*]

[a] Optics and Thermal Radiation Research Center, Institute of Frontier and Interdisciplinary Science, Shandong University, Qingdao 266237, China
[b] School of Information Science and Engineering, Shandong University, Qingdao 266237, China
[c] School of Energy and Power Engineering, Shandong University, Jinan 250061, China
[d] School of Energy Science and Engineering, Harbin Institute of Technology, Harbin 150001, China

ARTICLE INFO

Keywords:
Transition probabilities
Partition function
PN

ABSTRACT

Transition properties for the $A^1\Pi$-$X^1\Sigma^+$ system of PN have been investigated. Three sets of the potential energy curves (PECs) for the $X^1\Sigma^+$ and $A^1\Pi$ states are studied by the *ab initio* calculation, the Rydberg-Klein-Rees method and an empirical fitting to the experimental energies. Transition probabilities are then computed utilizing the empirical PECs and a high-level *ab initio* transition dipole moment. The partition functions for temperatures up to 10000 K are generated by employing the hybrid empirical and *ab initio* energies of eight low-lying states. Finally, the line list of PN $A^1\Pi$-$X^1\Sigma^+$ transition is presented.

1. Introduction

PN is the first P-bearing molecule to be astronomically observed by Turner and Bally [1] and Ziurys [2] in Orion KL, Sagittarius B2 and W51. In the past ten years or so, PN has been observed in the circumstellar envelops of evolved stars [3], the star forming regions [4], the oxygen-rich AGB star IK Tauri [5], the massive dense cores [6], the solar-type star-forming regions [7], the oxygen-rich circumstellar envelopes [8], the Galactic Center [9], the Class I low-mass protostar B1 [10], the diffuse and translucent clouds [11]. Hence, spectral information of PN is very important in the characterization of these astronomical environments. Many experimental observations and theoretical calculations have been conducted in order to obtain more information about the spectroscopy of PN. Qin et al. [12] presented a detailed description of the history of the experimental observations and theoretical calculations for PN. Here we just gave a brief summary. Experimentally, except for the microwave spectrum generated from the ground state of PN, the $A^1\Pi$-$X^1\Sigma^+$ and $E^1\Sigma^+$-$X^1\Sigma^+$ spectra have been observed in the laboratory, together with the vacuum ultraviolet spectra generated from four higher electronic transitions. Most of the theoretical calculations concentrate on the electronic structures of PN, including potential energies and spectroscopic parameters. *Ab initio* methods [12,13] have been used to predict the dipole-allowed electronic transition properties of PN and the results have shown that four electronic transition systems, i.e., the $A^1\Pi$-$X^1\Sigma^+$, $E^1\Sigma^+$-$X^1\Sigma^+$, $2^1\Pi$-$X^1\Sigma^+$ and $2^1\Pi$-$A^1\Pi$, are very intense in comparison with other dipole-allowed transitions below the atomic dissociation limit of the P (^2D_u) + N (^2D_u). Among these four electronic transitions, the $A^1\Pi$-$X^1\Sigma^+$ transition is predicted to be most intense [13], which may be the reason why the $A^1\Pi$-$X^1\Sigma^+$ system is firstly observed in the laboratory.

The PN $A^1\Pi$-$X^1\Sigma^+$ system exhibits remarkable spectrum in the ultraviolet band and has been investigated in previous experiments [14–20]. Some of the spectroscopic information about the PN $A^1\Pi$-$X^1\Sigma^+$ transition has been obtained, including the transition wavenumbers and rovibrational energies for the $X^1\Sigma^+$ and $A^1\Pi$ states. However, the transition probabilities, such as Einstein coefficients, absorption band oscillator strength and Franck-Condon factors, for the PN $A^1\Pi$-$X^1\Sigma^+$ system have not been studied in detail and a complete line list of PN $A^1\Pi$-$X^1\Sigma^+$ transition has not been available in the literature.

ExoMol has provided an accurate line list for rovibrational transitions of the ground state [21]. The aim of this work is to investigate the transition properties of the $A^1\Pi$-$X^1\Sigma^+$ system for PN. The state-of-the-art *ab initio* method, the Rydberg-Klein-Rees (RKR) method and an empirical method by fitting to the available experimental energies are used to produce the potential energy curves (PECs) of the $X^1\Sigma^+$ and $A^1\Pi$ states. Transition probabilities of the $A^1\Pi$-$X^1\Sigma^+$ system, including Einstein coefficients and absorption band oscillator strengths are computed by using the empirical PECs and an *ab initio* transition dipole moment (TDM) curve. These results are potential useful for some astrophysical applications, such as planetary atmospheres and interstellar clouds. In

* Corresponding author at: Optics and Thermal Radiation Research Center, Institute of Frontier and Interdisciplinary Science, Shandong University, Qingdao 266237, China.
E-mail address: liulinhua@sdu.edu.cn (L. Liu).

https://doi.org/10.1016/j.cplett.2021.139028
Received 19 April 2021; Received in revised form 25 August 2021; Accepted 5 September 2021
Available online 8 September 2021

Table 1
Effect on spectroscopic constants by the core-valence electron correction (denoted as "CV") and scalar relativistic correction (indicated as "DK") and extrapolation to the CBS limit using AV5Z and AV6Z basis sets (represented as "56") for the $X^1\Sigma^+$ and $A^1\Pi$ states at the icMRCI + Q level of theory.

	$X^1\Sigma^+$				$A^1\Pi$			
	T_e	R_e	ω_e	B_e	T_e	R_e	ω_e	B_e
AV5Z	0.0	1.498	1325.6	0.7795	39756.1	1.554	1105.4	0.7253
AV6Z	0.0	1.497	1328.9	0.7805	39788.1	1.553	1107.2	0.7266
56	0.0	1.495	1333.7	0.7818	39832.2	1.553	1109.7	0.7283
CV	0.0	1.492	1339.1	0.7849	40606.9	1.548	1107.2	0.7305
DK	0.0	1.495	1333.6	0.7821	39862.9	1.551	1107.3	0.7285
56 + CV + DK	0.0	1.492	1339.2	0.7853	40637.7	1.548	1104.8	0.7306
Expt.a	0.0	1.491b	1337.0	0.7865	39805.6	1.547	1103.0	0.7310

[a]The experimental values of the $X^1\Sigma^+$ state are from Cazzoli et al. [27] and those of the $A^1\Pi$ state are from Saraswathy & Krishnamurty [19].
[b]The R_e value of the $X^1\Sigma^+$ state is from Saraswathy & Krishnamurty [19].

Section 2, we present three sets of the PECs for the $X^1\Sigma^+$ and $A^1\Pi$ states of PN by using the three methods mentioned above. The empirical PEC of the $X^1\Sigma^+$ state is directly selected in the work of Yorke et al.[21] because this PEC is sufficiently accurate. Transition probabilities of the $A^1\Pi$-$X^1\Sigma^+$ system are given and analyzed in Section 3. In section 4, partition functions of PN are calculated at different temperatures. A set of temperature-dependent spectra of PN $A^1\Pi$-$X^1\Sigma^+$ system is shown in section 5. Finally, the conclusion is drawn in Section 6.

2. Potential energy curves

Three sets of PECs for the $X^1\Sigma^+$ and $A^1\Pi$ states of PN were produced in this work: an *ab initio* one named PEC-A; a RKR one named PEC-R which was obtained by the RKR method; an empirical PEC-E obtained by fitting the available experimental energy term values. These three PECs are discussed in the following sections.

2.1. The Ab initio PEC-A

The internally contracted multireference configuration-interaction, icMRCI, and underlying complete active space self-consistent field, CASSCF, calculations were performed using the aug-cc-pV6Z (AV6Z) basis set for both P and N atoms. To obtain more accurate potential energy, the basis extrapolation to the complete basis set (CBS) limit, electron correlation between core and valence electrons and scalar relativistic effect were considered. Basis extrapolation was considered by using the formula given by Truhlar [22] with the icMRCI/ aug-cc-pV5Z (AV5Z) and icMRCI/AV6Z potential energies. This formula is known to perform very well [12,23]. Electron correlation was taken into account via the icMRCI/cc-pCV5Z method with the P core (1*s*, 2*s* and 2*p*) and N core (1*s*) electrons correlated together with the valence electrons. Scalar relativistic effect was considered via third-order Douglas-Kroll-Hess (DKH3) Hamiltonian approximation at the icMRCI/cc-pV5Z-DK level of theory. Energies were computed in the internuclear distances from r = 1.05 to 10 Å. The intervals are 0.02 Å for the internuclear distances from 1.3 to 1.9 Å and 0.05 Å for other internuclear distances. Such calculations were performed using MOLPRO software package [24]. Detailed treatments can refer to Ref. [12], which investigated fifteen electronic transition bands.

Based on the calculated PECs of the $X^1\Sigma^+$ and $A^1\Pi$ states, the rovibrational energy levels are determined by the radial Schrödinger equation given by [25,26]

$$-\frac{\hbar^2}{2\mu}\frac{d^2\psi_{\upsilon J}(r)}{dr^2}+V_J(r)\psi_{\upsilon J}(r)=E_{\upsilon J}\psi_{\upsilon J}(r) \tag{1}$$

where μ is the reduced mass of the molecule, υ and J represent the vibrational and rotational quantum number, respectively, the effective potential $V_J(r)$ is a sum of a centrifugal term and the electronic potential. Such treatment is implemented in DUO [25]. The obtained rovibrational energy levels can be used to fit spectroscopic constants, including electronic excited energy T_e, equilibrium internuclear distance R_e, harmonic frequency ω_e, first-order anharmonic constant $\omega_e x_e$ and rotation constant B_e and rotation-vibration coupling constant α_e. Due to the negligible effects on the $\omega_e x_e$ and α_e by the core-valence electron correlation and scalar relativistic corrections and extrapolation to the CBS limit for the $X^1\Sigma^+$ and $A^1\Pi$ states at the icMRCI + Q level of theory, Table 1 only presents their effect on the T_e, R_e, ω_e and B_e. The T_e of the $A^1\Pi$ state is increased by 774.7 and 30.7 cm^{-1} with the core-valence electron correlation correction and scalar relativistic correction added, respectively. These two corrections make the T_e further to the experimental value. For the $X^1\Sigma^+$ state, core-valence electron correlation correction decreases R_e by 0.003 Å and increases ω_e and B_e by 5.4 cm^{-1} and 0.0031 cm^{-1}. Scalar relativistic correction makes R_e unchanged and increases ω_e and B_e by 0.1 cm^{-1} and 0.0003 cm^{-1}, respectively. For the $A^1\Pi$ state, core-valence electron correlation correction decreases R_e and ω_e by 0.005 Å and 2.5 cm^{-1}, respectively, and increases B_e by 0.0022 cm^{-1}. Scalar relativistic correction decreases R_e and ω_e by 0.002 Å and 2.4 cm^{-1}, respectively, and increases B_e by 0.0002 Å. These results show that the electron correlation between the core and valence shells is very important to accurately predict the vibrational and rotational energy levels. However, core-valence electron correlation gives a large prediction of the T_e value. It is worth noting that, almost certainly because of the consideration of the electron correlation between the core and valence electrons, scalar relativistic effect and basis extrapolation, good agreement with experiment is obtained for the *ab initio* PEC. Such treatment improves the electronic potential energy as exhibited as the fitted spectroscopic constants, which still exists large errors compared with the experimental ones (as shown in Table 1). One of the advantages of *ab initio* calculations is the good prediction of the trend of the PEC at longer internuclear distances.

2.2. The RKR PEC-R

The RKR method is a first-order semiclassical inversion procedure that is founded by Rydberg [28], Klein [29] and Ree [30] and is widely used for reconstructing the PEC of a diatomic molecule electronic state. The related formulae and derivation can refer to the RKR [31] and LEVEL [26] programs. The key conclusions of this method consist of two Klein integrals [31]

$$r_2(\upsilon)-r_1(\upsilon)=2\sqrt{\frac{\hbar^2}{2\mu}}\int_{\upsilon_{min}}^{\upsilon}\frac{d\upsilon'}{[G_\upsilon-G_{\upsilon'}]^{1/2}}=2f(\upsilon) \tag{2}$$

$$\frac{1}{r_1(\upsilon)}-\frac{1}{r_2(\upsilon)}=2\sqrt{\frac{2\mu}{\hbar^2}}\int_{\upsilon_{min}}^{\upsilon}\frac{B_{\upsilon'}d\upsilon'}{[G_\upsilon-G_{\upsilon'}]^{1/2}}=2g(\upsilon) \tag{3}$$

where $r_1(\upsilon)$ and $r_2(\upsilon)$ are inner and outer classical turning points of the PEC for a given vibrational level υ, μ is the reduced mass of the molecule, $\hbar$ is the reduced Planck's constant, υ_{min} is the non-integer effective value of the vibrational quantum number at the potential minimum, G_υ and B_υ

are the vibrational energy level and the inertial rotational constant, respectively.

These two Klein integrals are used to reconstruct the PECs near the equilibrium internuclear region corresponding to the experimental vibrational limit of spectroscopic constants. Beyond this internuclear region, the PEC is extrapolated by using a repulsive potential V_{rep}(r) for the shorter internuclear distance and a Hulburt and Hirschfelder potential V_{HH}(r) for the longer internuclear distance, as adopted by Chauveau et al. [32] and da Silva et al. [33]. These two theoretical potentials are given by

$$V_{rep}(r) = \frac{a_1}{r^{b_1}} \tag{4}$$

$$V_{HH}(r) = D_e\left[1 - e^{-a_2(r-r_e)}\right]^2 + D_e\left[b_2 a_2^3 (r-r_e)^3 e^{-2a_2(r-r_e)}(1 + a_2 c_2 (r - r_e))\right] \tag{5}$$

where D_e and r_e refer to the dissociation energy and the equilibrium internuclear distance, respectively, a_1, b_1, a_2, b_2 and c_2 are floating parameters that need to be adjusted to ensure continuity with the potential energy curve.

Several experimental investigations were carried out on the spectroscopic constants of the $X^1\Sigma^+$ and $A^1\Pi$ states [14,15,17–20]. Here, spectroscopic constants from Ghosh et al. [17] were chosen to reconstruct the PECs of the $X^1\Sigma^+$ and $A^1\Pi$ states by RKR method because they are valid for a relatively large coverage of vibrational energy levels, involving v = 0–11 for the $X^1\Sigma^+$ state and v = 0–10 for the $A^1\Pi$ state. Beyond the valid coverage of the vibrational energy levels, the PECs are extrapolated using a repulsive potential and a Hulburt and Hirschfelder potential mentioned above.

The RKR method can accurately reconstruct the PECs of a diatomic molecule for the internuclear distances which cover the experimental vibrational levels and hence has been used by many researchers [32,34,35].

2.3. The empirical PEC-E

Empirical potential fitting is an increasingly popular method that is adopted for refining or improving the *ab initio* or RKR PEC by using the experimental energy term values or wavenumbers [25,36]. The PEC of an electronic state for a diatomic molecule is often described by an Extended Morse Oscillator (EMO) function which has a formulism as follows [25]:

$$V(r) = V_e + D_e[1 - exp(-\beta_{\mathrm{EMO}}(r)(r - r_e))]^2, \tag{6}$$

where V_e is the electronic excitation energy, D_e is the dissociation energy, r_e is the equilibrium internuclear distance of a PEC, and β_{EMO} is the distance-dependent exponent coefficient, defined as

$$\beta_{\mathrm{EMO}}(r) = \sum_{k=0}^{N} B_k \xi_p^k$$

$$\xi_p = \frac{r^p - r_e^p}{r^p + r_e^p}.$$

where N is the expansion order parameter, p is an adjustable parameter.

The empirical PEC of the $X^1\Sigma^+$ state is directly selected from Yorke et al.[21]. In this work, we carried out a MARVEL (Measured Active Vibration Rotation Energy Levels) analysis of the experimental rovibrational transition wavenumbers for the $X^1\Sigma^+$ state. MARVEL is a well-developed procedure which can convert high-resolution experimental wavenumbers to empirical energy levels and uncertainties [37–40]. Finally, a self-consistent set of 61 empirical energy levels with their uncertainties for the $X^1\Sigma^+$ state was obtained and provided in the supplemental material. These empirical energy levels will be useful for high precision studies in astrophysics. Furthermore, the *ab initio* PEC for the $A^1\Pi$ state is refined by fitting the experimental energies from Ghosh et al. [17] and Sarashwathy et al. [19] as implement in DUO program [25].

Table 2
Fitting parameters of the empirical EMO potential of the $A^1\Pi$ electronic state for PN.

Parameters	PEC ($A^1\Pi$)
V_e (cm^{-1})	39806.0
r_e (Å)	1.547
D_e (cm^{-1})	41499.6
p	1
N_L	1
N_R	6
B_0	2.04974457535664
B_1	0.0678730087733480
B_2	−1.96516954373763
B_3	17.3510140920318

A total of 401 experimental rovibrational energies covers a maximum vibrational quantum number of 10 and a maximum rotational quantum number of 80 with estimated maximum uncertainties of 2 cm^{-1}, which are provided in the supplemental material. The fitting procedures are as follows. Firstly, the initial fitting parameters of the EMO function are obtained by fitting the *ab initio* PEC. Then, the obtained parameters are refined by fitting the experimental data to ensure more accurate PEC near the equilibrium internuclear distances. During such process, the *ab initio* PEC serves as a reference to ensure the accuracy of the long-range PEC. Also, a trial-and-error approach is often needed to ensure the accuracy of the fitting. DUO is a well-developed program to compute rotational, rovibrational and rovibronic spectra of diatomic molecules and has been successfully utilized to produce spectroscopic data for many diatomic molecules, including CaO [41], MgO [42] and CP [43], etc. DUO uses a grid-based sinc DVR method to solve the coupled Schrödinger equation. The grid of uniformly distributed 501 points from 1.1 to 4.0 Å was used in the calculations. This fit is highly non-linear and is normally done iteratively by considering just one electronic or vibronic state at a time. Further details of the fitting procedure can refer to the related publications [25,44]. During the fit, the refined PEC of the $A^1\Pi$ state is described by Eqs. (5)–(6). The fitted parameters are listed in Table 2. Fig. 1(a) displays the absolute values of the residuals between the experimentally derived and fitted energy term values for the $A^1\Pi$ state. The root-mean-square error (RMSD) value is 1.23 cm^{-1}. An agreement within 10 cm^{-1} (<0.03%) can be observed for the wavenumber range from 40,000 to 50000 cm^{-1}.

Fig. 1(b) compares the empirical PEC-E with an *ab initio* PEC-A and a RKR PEC-R. Due to the lack of experimental data for energies higher than 50000 cm^{-1}, only the range $R \approx$ 1.38–1.82 Å of the empirical PEC-E is accurately described, as well as the RKR PEC-R. Within this range, PEC-R and PEC-E agree to about 5 cm^{-1}. Outside it, the two PECs differ significantly. However, the PEC-E shows better agreement with the PEC-A than PEC-R at larger internuclear distances. Moreover, the energy term values obtained with the PEC-R and PEC-E are very close (see Table 3) for small internuclear distances corresponding to $v \leq 11$. Hence, the PEC-E is adopted to compute the transition probabilities as shown below.

3. Transition probabilities

The radial eigenfunctions $\psi_{v,J}(r)$ can be determined by solving the radial Schrödinger equation [Eq. (1)].Wave functions were then combined with TDM curve to calculate the transition probabilities of the $A^1\Pi$-$X^1\Sigma^+$ system as implemented in DUO [25].

For many applications, the Einstein A coefficient is an important intermediate quantity to compute the spectral intensity of a transition and is defined as follows [26]

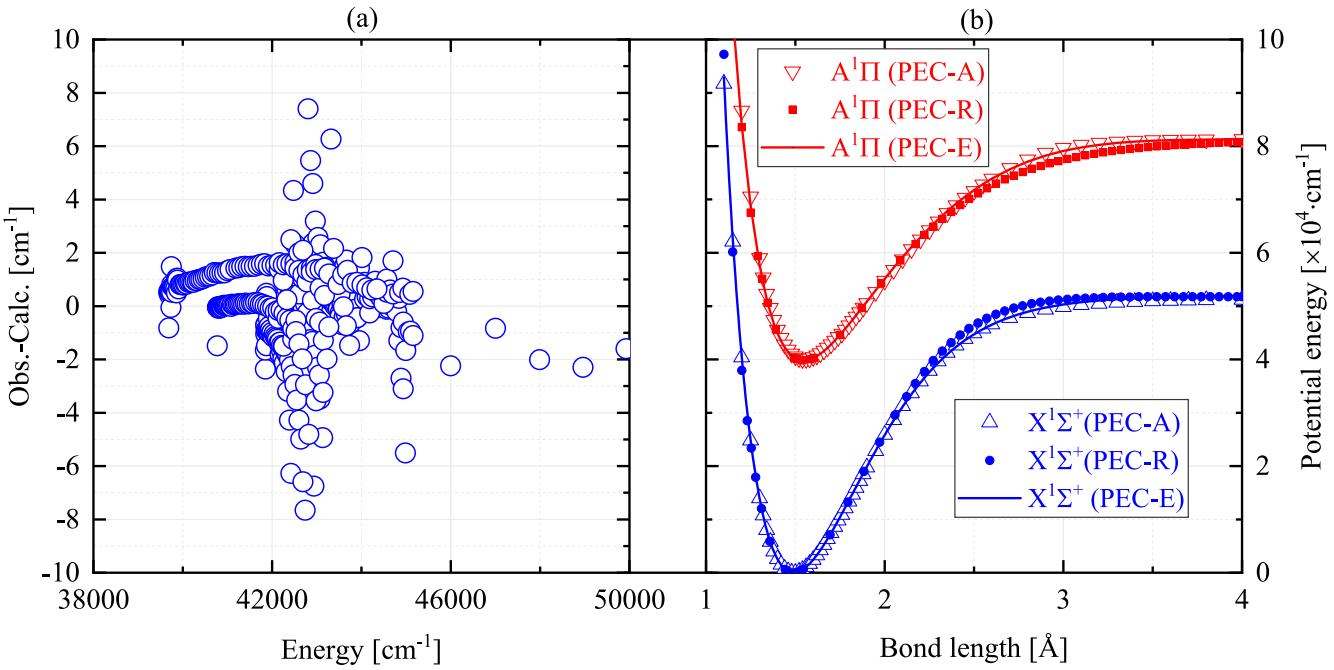

Fig. 1. (a) Accuracy of the fit: the absolute values of the residuals between the experimentally derived (obs.) and calculated (calc.) energy term values from empirical PEC (PEC-E) of the $A^1\Pi$ state. (b) The PECs for the $X^1\Sigma^+$ and $A^1\Pi$ states of PN: *ab initio* ones (PEC-A) are obtained at the icMRCI + Q level of theory with the consideration of the core-valence electron correlation, scalar relativistic effect and basis set extrapolation; The RKR ones (PEC-R) are obtained by RKR method; The empirical potential of the $X^1\Sigma^+$ state is directly selected from York et al. [21] and the empirical potential of the $A^1\Pi$ state is obtained by fitting the experimental energies [17,19].

Table 3
Comparison between experimental vibrational term values ('obs.') and calculated ones ('Calc.') for three PECs of the $X^1\Sigma^+$ and $A^1\Pi$ states for PN. A represents the *ab initio* curve obtained at the icMRCI + Q/56 + CV + DK level of theory; R indicates a reconstructed curve by RKR method; E is an empirical curve defined by Eq. (5). The calculated vibrational energy values for the $X^1\Sigma^+$ state are from York et al. [21]. Experimental energy terms are from Ghosh et al. [17]. The vibrational energy term values for A, R and E are all obtained based on experimental electronic excitation energy T_e ($A^1\Pi$) = 39805.6 cm^{-1} for comparison.

υ	$X^1\Sigma^+$				$A^1\Pi$			
	Obs.	Calc.			Obs.	Calc.		
		A	R	E		A	R	E
0	0.00	0.00	0.00	0.00	39688.56	39678.90	39688.55	39689.38
1	1323.17	1326.23	1323.58	1323.15	40777.12	40759.19	40777.39	40778.62
2	2632.50	2638.94	2633.22	2632.44	41850.60	41824.61	41851.68	41852.96
3	3927.87	3934.88	3928.98	3927.85	42912.56	42872.87	42911.46	42912.54
4	5209.47	5216.84	5210.78	5209.35	43956.15	43897.29	43956.70	43957.46
5	6477.04	6487.16	6478.66	6476.90	44986.20	44889.98	44987.44	44987.83
6	7730.63	7742.11	7732.56	7730.45	46001.37	45867.41	46003.65	46003.75
7	8970.23	8978.50	8972.48	8969.95	47004.22	46859.51	47005.36	47005.35
8	10195.72	10194.67	10198.40	10195.34	47990.19	47838.61	47992.54	47992.73
9	11406.64	11388.41	11410.29	11406.56	48962.86	48793.16	48965.22	48966.00
10	12603.89	12567.72	12608.14	12603.53	49922.40	49750.72	49923.38	49925.25
11	13786.95	13747.32	13791.92	13786.18				

$$A_{\upsilon' J' \upsilon'' J''} = 3.1361891 \times 10^{-7} \frac{S(J', J'')}{2J' + 1} \times \nu^3_{\upsilon' J' \upsilon'' J''} R^2_{\upsilon' J' \upsilon'' J''} \quad (9)$$

here, S (J', J'') is the Hönl-London rotational intensity factor, $R^2_{\upsilon' J' \upsilon'' J''}$ is the transition dipole moment matrix element, which can be expressed as

$$R_{\upsilon' J' \upsilon'' J''} = |\langle \psi_{\upsilon' J'}(r) | M(r) | \psi_{\upsilon'' J''} \rangle| \quad (10)$$

where $M(r)$ is the TDM.

The absorption band oscillator strengths can be obtained from the expression

$$f_{\upsilon' J' \upsilon'' J''} = 4.703 \times 10^{-7} \nu_{\upsilon' J' \upsilon'' J''} \frac{S(J', J'')}{2J'' + 1} R^2_{\upsilon' J' \upsilon'' J''} \quad (11)$$

Here, the variables are identical with Eq. (9). The relationship between the line and band oscillator strengths is

$$f_{\upsilon' \upsilon''} = f_{\upsilon' J' \upsilon'' J''} \frac{\nu_{\upsilon' \upsilon''}}{\nu_{\upsilon' J' \upsilon'' J''}} g \frac{2J'' + 1}{S(J', J'')} \quad (12)$$

where, g is the statistical weight factor, which can be calculated by

$$g = \frac{2 - \delta_{(0,\Lambda')} \delta_{(0,\Lambda'')}}{2 - \delta_{(0,\Lambda')}} \quad (13)$$

where, δ is the Kronecker delta, Λ' and Λ'' are the projections of the electronic orbital angular momentum on the internuclear axis for the upper and lower electronic levels, respectively.

In this work, the empirical PEC-E and TDM from Qin et al. [12] calculated at the icMRCI/AV6Z level of theory are as an input into DUO

Table 4
Einstein A coefficients (first line, in s^{-1}) and absorption band oscillator strengths (second line) for $A^1\Pi$-$X^1\Sigma^+$ transition bands, 9.0302E + 05 represents 9.0302×10^5.

v'	v''											
	0	1	2	3	4	5	6	7	8	9	10	11
0	9.0302E + 05	4.0967E + 05	9.1445E + 04	1.3041E + 04	1.2617E + 03	6.7501E + 01	1.1088E + 00	3.1984E-01	4.2233E-01	1.5330E-02	1.9471E-01	8.3005E-03
	1.6972E-03	8.2835E-04	1.9917E-04	3.0636E-05	3.2014E-06	1.8524E-07	3.2959E-09	1.0312E-09	1.4792E-09	5.8416E-11	8.0844E-10	3.7609E-11
1	6.0989E + 05	1.7196E + 05	4.3889E + 05	1.9370E + 05	4.1490E + 04	5.2731E + 03	4.0482E + 02	2.3769E + 01	2.8160E + 00	2.9241E-02	5.4147E-01	7.8118E-02
	1.0544E-03	3.1885E-04	8.7378E-04	4.1454E-04	9.5560E-05	1.3086E-05	1.0838E-06	6.8732E-08	8.8064E-09	9.9016E-11	1.9879E-09	3.1131E-10
2	2.2694E + 05	6.1023E + 05	1.8652E + 02	3.0133E + 05	2.5794E + 05	8.1216E + 04	1.3911E + 04	1.4250E + 03	9.0011E + 01	3.1738E + 00	3.7413E-01	1.5751E + 00
	3.6255E-04	1.0427E-03	3.4123E-07	5.9078E-04	5.4251E-04	1.8343E-04	3.3774E-05	3.7229E-06	2.5332E-07	9.6315E-09	1.2255E-09	5.5747E-09
3	6.1259E + 04	4.3913E + 05	3.8785E + 05	6.9496E + 04	1.4261E + 05	2.7110E + 05	1.2463E + 05	2.7563E + 04	3.3582E + 03	2.0454E + 02	7.8756E-01	6.2536E + 00
	9.0828E-05	6.9465E-04	6.5514E-04	1.2546E-04	2.7538E-04	5.6048E-04	2.7609E-04	6.5487E-05	8.5649E-06	5.6043E-07	2.3203E-09	1.9826E-08
4	1.3190E + 04	1.8090E + 05	5.3441E + 05	1.5894E + 05	1.8214E + 05	3.5621E + 04	2.3561E + 05	1.5989E + 05	4.4769E + 04	6.1418E + 03	2.9715E + 02	1.8961E + 00
	1.8222E-05	2.6602E-04	8.3716E-04	2.6543E-04	3.2453E-04	6.7761E-05	4.7889E-04	3.4750E-04	1.0412E-04	1.5295E-05	7.9295E-07	5.4252E-09
5	2.3744E + 03	5.4026E + 04	3.1976E + 05	5.0057E + 05	2.6176E + 04	2.4536E + 05	2.2451E + 01	1.6852E + 05	1.7678E + 05	6.1518E + 04	9.3015E + 03	4.7822E + 02
	3.0673E-06	7.4137E-05	4.6640E-04	7.7661E-04	4.3224E-05	4.3152E-04	4.2079E-08	3.3682E-04	3.7702E-04	1.4008E-04	2.2625E-05	1.2432E-06
6	3.8004E + 02	1.2651E + 04	1.2663E + 05	4.3701E + 05	3.7278E + 05	2.9874E + 03	2.3699E + 05	2.4955E + 04	9.2646E + 04	1.7056E + 05	7.6747E + 04	1.4509E + 04
	4.6063E-07	1.6257E-05	1.7261E-04	6.3233E-04	5.7285E-04	4.8782E-06	4.1145E-04	4.6089E-05	1.8212E-04	3.5701E-04	1.7113E-04	3.4479E-05
7	5.8256E + 01	2.4062E + 03	3.8265E + 04	2.2349E + 05	4.9555E + 05	2.1579E + 05	5.3615E + 04	1.7615E + 05	8.1833E + 04	3.4295E + 04	1.5207E + 05	9.4839E + 04
	6.6455E-08	2.9049E-06	4.8916E-05	3.0267E-04	7.1134E-04	3.2847E-04	8.6587E-05	3.0195E-04	1.4895E-04	6.6311E-05	3.1245E-04	2.0713E-04
8	7.7813E + 00	4.0515E + 02	9.1734E + 03	8.3317E + 04	3.2961E + 05	4.7946E + 05	8.4849E + 04	1.3004E + 05	9.2785E + 04	1.3108E + 05	5.4807E + 03	1.2876E + 05
	8.3784E-09	4.6094E-07	1.1032E-05	1.0596E-04	4.4351E-04	6.8285E-04	1.2796E-04	2.0773E-04	1.5705E-04	2.3517E-04	1.0425E-05	2.5972E-04
9	4.6960E-01	7.1561E + 01	1.7482E + 03	2.4684E + 04	1.4984E + 05	4.2083E + 05	3.9545E + 05	1.3223E + 04	1.9496E + 05	2.4812E + 04	1.4960E + 05	8.6715E + 02
	4.7857E-10	7.6938E-08	1.9838E-06	2.9573E-05	1.8961E-04	5.6266E-04	5.5884E-04	1.9757E-05	3.0808E-04	4.1475E-05	2.6458E-04	1.6229E-06
10	2.6839E-03	1.2478E + 01	2.8433E + 02	5.8938E + 03	5.2883E + 04	2.3276E + 05	4.7562E + 05	2.7401E + 05	2.8883E + 03	2.1445E + 05	1.5261E + 02	1.4539E + 05
	2.5953E-12	1.2711E-08	3.0526E-07	6.6709E-06	6.3122E-05	2.9308E-04	6.3193E-04	3.8426E-04	4.2761E-06	3.3525E-04	2.5194E-07	2.5351E-04

Table 5
Comparison between the calculated Franck-Condon factors (first row) and the experimental ones (second row) [45].

v'	v''				
	0	1	2	3	4
0	0.5619	0.3185	0.0869	0.0148	0.0018
	0.58	0.31	0.08	0.02	
1	0.3065	0.1040	0.3358	0.1816	0.0476
	0.38	0.15	0.32	0.14	0.07

to calculate the transition probabilities. Our calculated Einstein A coefficients and absorption band oscillator strengths including $v' = 0$–10 → $v'' = 0$–11 transition bands are listed in Table 4. Larger Einstein coefficients are located in and near the diagonal area, and the largest value (9.0302×10^5 s^{-1}) corresponds to strong transition v'=0 → v''=0. A set of line list for the $A^1\Pi$-$X^1\Sigma^+$ transition covering vibrational levels v' and v'' up to 50 is given in the supplemental material. For comparison with the experimental transition probabilities, the Franck-Condon factors $q_{v'v''}$ were calculated by

$$q_{v'v''} = \left(\int \psi_{v'}(r)\psi_{v''}(r)dr \right)^2$$

The computed Franck-Condon factors for v'=0, 1 → v''=0–4 transition bands are listed in Table 5, together with the experimental ones. Obviously, good agreement has been observed.

4. Partition function

The partition function for PN was computed using the EXOCROSS program [46]. The formula is given

$$Q(T) = \sum_n g_{ns}(2J_n + 1)e^{c_2\widetilde{E}_n}/T \quad (15)$$

where g_{ns} is the nuclear-spin statistical factor, c_2 (=hc/k_B) is the second radiation constant (cm·K), T is the temperature (K) and $\widetilde{E}_n$(=E_n/hc) is the energy term value (cm^{-1}). In the process of computing the partition function of PN, the empirical PEC-E for the $X^1\Sigma^+$ and $A^1\Pi$ states, and the icMRCI + Q/56 + CV + DK PECs for the $a^3\Sigma^+$, $d^3\Delta$, $b^3\Pi$, $e^3\Sigma^-$, $C^1\Sigma^-$ and $D^1\Delta$ states from Qin et al. [12] are considered and as an input into DUO to calculate the energy term values. The maximum vibrational quantum numbers of 50, 40, 40, 30, 40, 50, 50 and 50 for the $X^1\Sigma^+$, $a^3\Sigma^+$, $d^3\Delta$, $b^3\Pi$, $e^3\Sigma^-$, $C^1\Sigma^-$, $A^1\Pi$ and $D^1\Delta$ states, respectively, and a maximum rotational quantum of 200 for each vibrational energy level were considered. The nuclear statistical weight of PN is $g_{ns} = 4$. The maximum

Table 6
Comparison of the calculated partition function with previous calculations.

T	This work	Barklem and Collet [47]	York et al. [21]	Irwin [48]
100	356.2	356.2	356.2	515.6
200	711.2	711.2	711.2	848.3
300	1068.2	1068.2	1068.2	1156.7
500	1817.9	1817.9	1817.9	1848.6
700	2666.1	2666.2	2666.1	2676.0
1000	4188.4	4188.4	4188.4	4190.8
2000	11717.7	11717.6	11717.8	11719.8
3000	23230.0	23227.8	23229.7	23215.1
4000	38927.4	38898.0	38905.7	38824.1
5000	59190.7	58913.6	58936.7	58719.8
6000	84999.0	83494.4		
7000	118437.1	112926.0		
8000	162979.1	147604.4		
9000	223380.8	188074.0		
10,000	305251.9	235051.6		

temperature was set to 10000 K and the partition function was determined in increments of 1 K. Table 6 presents partition function values at selected temperatures and a comparison with previous studies. At low temperatures below 3000 K, our partition function is in good agreement with that of Barklem and Collet [47] and York et al. [21]. At temperatures from 3000 to 5000 K, our partition function is a little higher than that of Barklem and Collet [47], York et al. [21] and Irwin [48]. At temperatures from 5000 to 10000 K, our partition function is much higher than that of Barklem and Collet [47], which may be due to more electronic states considered in this work. The full tabulation of partition function for PN is given in the supplementary material.

5. Simulated spectra

The line list of the $A^1\Pi$-$X^1\Sigma^+$ system was then used to compute various absorption spectra in the form of integrated cross-sections as implemented in the EXOCROSS program [46]. The absorption line intensity I_{fi} (cm·molecule^{-1}) for a spectral transition $f \leftarrow i$ is given by [46]

$$I(f \leftarrow i) = \frac{g_f^{\mathrm{tot}} A_{fi}}{8\pi c \nu_{fi}^2} \frac{e^{-c_2 \widetilde{E}_i}/T\left(1 - e^{-c_2 \nu_{fi}/T}\right)}{Q(T)} \tag{16}$$

where $g_f^{\mathrm{tot}}$is the total degeneracy of f state, $Q(T)$ is the partition function given in Eq. (15). The cross section $\sigma_{fi}(\nu)$ for a transition $f \leftarrow i$ is related to the absorption line intensity, given by

$$I_{fi} = \int_{-\infty}^{\infty} \sigma_{fi}(\nu) d\nu \tag{17}$$

Based on the calculated line lists, the cross-sections for PN $A^1\Pi$-$X^1\Sigma^+$ transition are computed. Fig. 2 displays the temperature-dependent $A^1\Pi$-$X^1\Sigma^+$ absorption spectrum of PN. The spectra are prominent in the near ultraviolet as observed in the experiment [14–20]. Phosphorus is one of the essential elements for life due to its central role in biochemical processes and P-containing molecules are of great interest in astronomy [9,11,49,50]. Such spectra can be used to identify the presence of PN in the interstellar environment and to model non-astrophysical detection applications, such as PN-containing plasmas.

6. Discussion and conclusion

We presented three sets of PECs for the $X^1\Sigma^+$ and $A^1\Pi$ states of PN: an *ab initio* PEC-A, a RKR PEC-R and an empirical PEC-E. The *ab initio* PEC-A is obtained by the icMRCI method together with the Davidson, core-valence electron correlation and scalar relativistic corrections, as well as the basis set extrapolation. The RKR PEC-R is obtained by the RKR method along with the theoretical extrapolation potentials. The empirical PEC-E is obtained by fitting to available experimental energy terms. Comparisons shows that the PEC-E is more accurate than the other two curves. Hence, the empirical PECs and the TDMs calculated by icMRCI/AV6Z method are used to compute transition probabilities (comprising Einstein A coefficients, Franck-Condon factors and absorption band oscillator strengths) of the $A^1\Pi$-$X^1\Sigma^+$ system for PN. The Franck-Condon factors are consistent with the experimental determinations. A set of line list for the $A^1\Pi$-$X^1\Sigma^+$ transition covering vibrational levels v' and v'' up to 50 is given in the supplemental material. It can be seen that our results

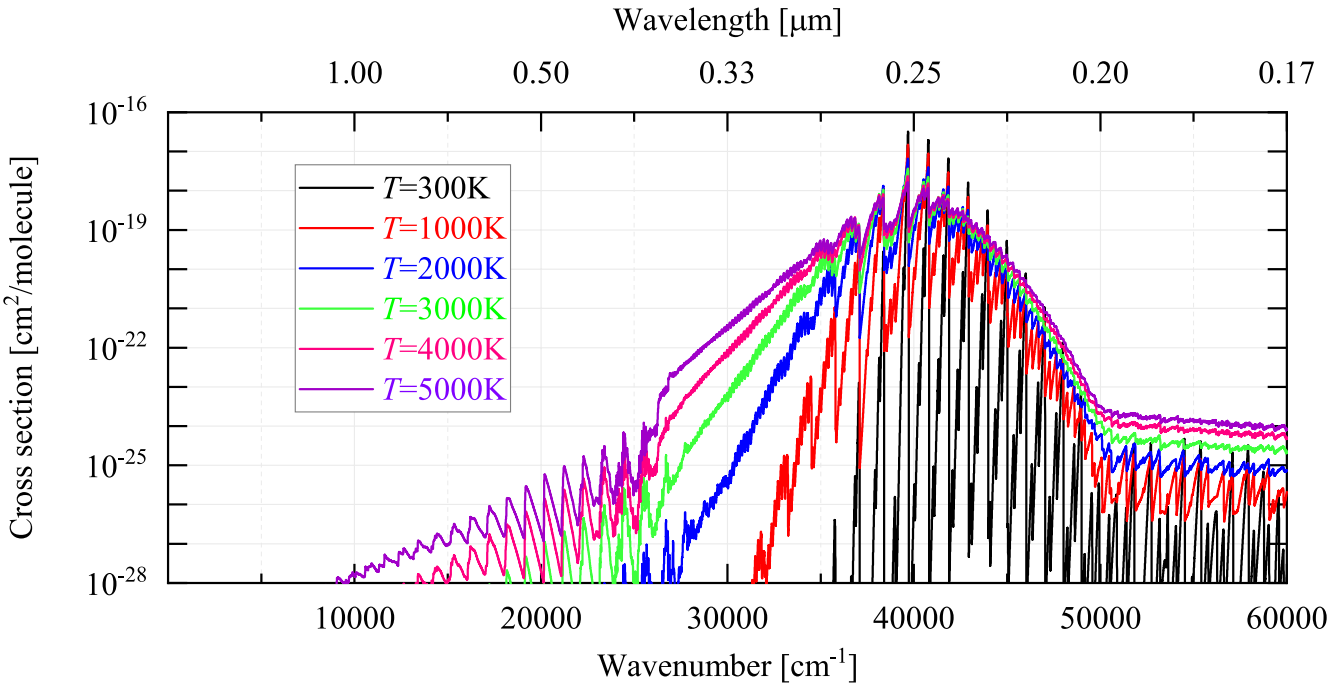

Fig. 2. Temperature dependence of PN cross sections obtained by using the line list of the $A^1\Pi$-$X^1\Sigma^+$ transition and a Gaussian profile with a HWHM = 10 cm^{-1}, from bottom to top: T = 300, 1000, 2000, 3000, 4000 and 5000 K.

of transition wavenumbers in agreement with experimental measurements. Therefore, we expect that our theoretical calculations are credible and can be useful to predict the spectral characteristics, especially those not observed in the experiments. Moreover, partition functions for temperatures up to 10000 K are generated by employing the hybrid empirical energies of the $X^1\Sigma^+$ and $A^1\Pi$ states and *ab initio* energies of the $a^3\Sigma^+$, $d^3\Delta$, $b^3\Pi$, $e^3\Sigma^-$, $C^1\Sigma^-$ and $D^1\Delta$ states. Our partition function shows good agreement with previous work done by Barklem and Collet [47] and York et al. [21] at temperatures below 3000 K, exhibits a little higher at temperatures from 3000 to 5000 K and displays much higher at temperatures from 5000 to 10000 K. Our partition functions are theoretically valid because we consider more electronic states.

We hope that our theoretical work can be significantly helpful for further study of PN. It can be used for the analysis of some experimentally measured spectra, especially the rovibrational transitions of large Δv or high overtone bands. It comes true that spectral transition properties of PN $A^1\Pi$-$X^1\Sigma^+$ system are applied not only at low temperatures, but also at high temperatures to characterize some astrophysical environments such as hot planetary atmospheres.

Future work is required to calculate the lines by considering the effects of the perturbations of the $A^1\Pi$ state by adjacent electronic states. Including perturbations should result in better line positions and line intensities. Isotopologues of PN also require the similar type calculations for the completement of the interstellar abundance PN line list.

7. Supplemental material

The line lists for the $A^1\Pi$-$X^1\Sigma^+$ transition are provided here. The considered maximum vibrational quantum numbers are 50 and 50 for the $X^1\Sigma^+$ and $A^1\Pi$ states with a maximum rotational quantum number of 200. The line lists are given in the ExoMol format, including the .states and .trans files. MARVEL input and output are also provided, along with the partition function. Supplemental data are available in the zip file of supplemental material.

CRediT authorship contribution statement

Zhi Qin: Conceptualization, Investigation, Data curation, Writing – original draft, Writing – review & editing. **Tianrui Bai:** Investigation, Visualization. **Linhua Liu:** Supervision, Funding acquisition, Data curation, Project administration, Writing – review & editing.

Declaration of Competing Interest

The authors declare that they have no known competing financial interests or personal relationships that could have appeared to influence the work reported in this paper.

Acknowledgement

This work is sponsored by the National Natural Science Foundation of China under Grant NO. 51421063. This work is also supported by the Postdoctoral Applied Research Project of Qingdao. The scientific calculations in this paper have been done on the HPC Cloud Platform of Shandong University.

Appendix A. Supplementary material

Supplementary data to this article can be found online at https://doi.org/10.1016/j.cplett.2021.139028.

References

[1] B.E. Turner, J. Bally, Detection of interstellar PN: the first identified phosphorus compound in the interstellar medium, Astrophys. J. 321 (1987) L75–L79, https://doi.org/10.1086/185009.
[2] L.M. Ziurys, Detection of interstellar PN: the first phosphorus-bearing species observed in molecular clouds, Astrophys. J. 321 (1987) L81, https://doi.org/10.1086/185010.
[3] S.N. Milam, D.T. Halfen, E.D. Tenenbaum, A.J. Apponi, N.J. Woolf, L.M. Ziurys, Constraining phosphorus chemistry in carbon- and oxygen-rich circumstellar envelopes: Observations of PN, HCP, and CP, Astrophys. J. 684 (2008) 618–625, https://doi.org/10.1086/589135.
[4] F. Fontani, V. Rivilla, F. van der Tak, C. Mininni, M. Beltrán, P. Caselli, Origin of the PN molecule in star-forming regions: the enlarged sample, Mon Not Roy. Astron. Soc. 489 (2019) 4530–4542, https://doi.org/10.1093/mnras/stz2446.
[5] E.D. Beck, T. Kamiński, N.A. Patel, K.H. Young, C.A. Gottlieb, K.M. Menten, L. Decin, PO and PN in the wind of the oxygen-rich AGB star IK Tau, Astron. Astrophys. 558 (2013) 132–140, https://doi.org/10.1051/0004-6361/201321349.
[6] F. Fontani, V.M. Rivilla, P. Caselli, A. Vasyunin, A. Palau, Phosphorus-bearing molecules in massive dense cores, Astrophys. J. 822 (2016) L30, https://doi.org/10.3847/2041-8205/822/2/L30.
[7] B. Lefloch, C. Vastel, S. Viti, I. Jimenezserra, C. Codella, L. Podio, C. Ceccarelli, E. Mendoza, et al., Phosphorus-bearing molecules in solar-type star-forming regions: first PO detection, Mon. Not. Roy. Astron. Soc. 462 (2016) 3937–3944, https://doi.org/10.1093/mnras/stw1918.
[8] L.M. Ziurys, D.R. Schmidt, J.J. Bernal, New circumstellar sources of PO and PN: the increasing role of phosphorus chemistry in oxygen-rich stars, Astrophys J. 856 (2018) 169, https://doi.org/10.3847/1538-4357/aaafc6.
[9] V.M. Rivilla, I. Jiménezserra, S. Zeng, S. Martín, J. Martínpintado, J. Armijosabendaño, S. Viti, R. Aladro, et al., Phosphorus-bearing molecules in the Galactic Center, Mon. Not. Roy. Astron. Soc. 475 (2018) L30–L34, https://doi.org/10.1093/mnrasl/slx208.
[10] J.B. Bergner, K.I. Öberg, S. Walker, V.V. Guzmán, T.S. Rice, E.A. Bergin, Detection of Phosphorus-bearing Molecules toward a Solar-type Protostar, Astrophys J Lett. 884 (2019) L36, https://doi.org/10.3847/2041-8213/ab48f9.
[11] J. Chantzos, V.M. Rivilla, A. Vasyunin, E. Redaelli, L. Bizzocchi, F. Fontani, P. Caselli, The first steps of interstellar phosphorus chemistry, A & A 633 (2020) A54, https://doi.org/10.1051/0004-6361/201936531.
[12] Z. Qin, J. Zhao, L. Liu, Energy levels, transition dipole moment, transition probabilities and radiative lifetimes for low-lying electronic states of PN, J Quant Spectrosc Radiat Transf. 227 (2019) 47–56, https://doi.org/10.1016/j.jqsrt.2019.02.002.
[13] K. Abbiche, M. Salah, K. Marakchi, O.K. Kabbaj, N. Komiha, Ab initio study of PN electronic states: a qualitative interpretation of the perturbation and predissociation effects on observed transitions, Mol. Phys. 112 (2014) 117–126, https://doi.org/10.1080/00268976.2013.804216.
[14] J. Curry, L. Herzberg, G. Herzberg, Spektroskopischer Nachweis und Struktur des PN-Moleküls, Zeitschrift Für Physik. 86 (1933) 348–366, https://doi.org/10.1007/BF01330645.
[15] J. Curry, L. Herzberg, G. Herzberg, Spectroscopic evidence for the molecule PN, J. Chem. Phys. 1 (1933) 749, https://doi.org/10.1063/1.1749238.
[16] P.N. Ghosh, A.C. Datta, Das Bandenspektrum des Phosphornitrids, Zeitschrift Für Physik. 87 (1934) 500–504, https://doi.org/10.1007/BF01333259.
[17] S.N. Ghosh, R.D. Verma, J. Vanderlinde, A high resolution study of A1Π-X1Σ transition of the PN molecule, Can. J. Phys. 59 (1981) 1640–1652, https://doi.org/10.1139/p81-216.
[18] P. Saraswathy, G. Krishnamurty, Isotope shifts in the A1Π-X1Σ+ system of PN molecule, Pramana. 23 (1984) 665–669, https://doi.org/10.1007/BF02846689.
[19] P. Saraswathy, G. Krishnamurty, Rotational analysis of $A^1\Pi$-$X^1\Sigma^+$ bands of $P^{14}N$ and $P^{15}N$: Perturbatio studies in the $A^1\Pi$ state, Pramana 29 (1987) 53–77, https://doi.org/10.1007/BF02845678.
[20] A.C. Le Floch, F. Melen, I. Dubois, H. Bredohl, A new study of the perturbations in the A1Π State of PN, J. Mol. Spectrosc. 176 (1996) 75–84, https://doi.org/10.1006/jmsp.1996.0063.
[21] L. Yorke, S.N. Yurchenko, L. Lodi, J. Tennyson, Exomol molecular line lists – VI, A high temperature line list for phosphorus nitride, Mon Not Roy Astron Soc. 445 (2014) 1383–1391, https://doi.org/10.1093/mnras/stu1854.
[22] D.G. Truhlar, Basis-set extrapolation, Chem. Phys. Lett. 294 (1998) 45–48, https://doi.org/10.1016/S0009-2614(98)00866-5.
[23] J.M. Wang, J.F. Sun, D.H. Shi, Accurate ab initio study of low-lying electronic states of phosphorus nitride radical, Chin. Phys. B 19 (2010) 340–346, https://doi.org/10.1088/1674-1056/19/11/113404.
[24] H.J. Werner, P.J. Knowles, G. Knizia, F.R. Manby, a. others, MOLPRO 2015, a package of ab initio programs, see http://wwwmolpronet..
[25] S.N. Yurchenko, L. Lodi, J. Tennyson, A.V. Stolyarov, Duo: a general program for calculating spectra of diatomic molecules, Comput. Phys. Commun. 202 (2016) 262–275, https://doi.org/10.1016/j.cpc.2015.12.021.
[26] R.J. Le Roy, LEVEL: A computer program for solving the radial Schrödinger equation for bound and quasibound levels, J Quant Spectrosc Radiat Transf. 186 (2017) 167–178, https://doi.org/10.1016/j.jqsrt.2016.05.028.
[27] G. Cazzoli, L. Cludi, C. Puzzarini, Microwave spectrum of $P^{14}N$ and $P^{15}N$: Spectroscopic constants and molecular structure, J. Mol. Struct. 780 (2006) 260–267, https://doi.org/10.1016/j.molstruc.2005.07.010.
[28] R. Rydberg, Graphische Darstellung einiger bandenspektroskopischer Ergebnisse, J. Ztschrift Für Physik. 73 (1932) 376–385, https://doi.org/10.1007/BF01341146.
[29] O. Klein, Zur Berechnung von Potentialkurven für zweiatomige Moleküle mit Hilfe von Spektraltermen, J. Ztschrift Für Physik. 76 (1932) 226–235, https://doi.org/10.1007/BF01341814.
[30] G.A.L. Rees, The calculation of potential-energy curves from band-spectroscopic data, Pub Astron Soc. 59 (1947) 998, https://doi.org/10.1088/0959-5309/59/6/310.

[31] R.J. Le Roy, RKR1: A computer program implementing the first-order RKR method for determining diatomic molecule potential energy functions, J Quant Spectrosc Radiat Transf. 186 (2017) 158–166, https://doi.org/10.1016/j.jqsrt.2016.03.030.
[32] S. Chauveau, M.Y. Perrin, P. Rivière, A. Soufiani, Contributions of diatomic molecular electronic systems to heated air radiation, J Quant Spectrosc Radiat Transf. 72 (2002) 503-30. 10.1016/S0022-4073(01)00141-8.
[33] M.L. da Silva, V. Guerra, J. Loureiro, P.A. Sá, Vibrational distributions in N2 with an improved calculation of energy levels using the RKR method, Chem. Phys. Lett. 348 (2008) 187–194, https://doi.org/10.1016/j.chemphys.2008.02.048.
[34] C.O. Laux, C.H. Kruger, Arrays of radiative transition probabilities for the N_2 first and second positive, NO β and γ, N_2^+ first negative, and O_2 Schumann-Runge band systems, J Quant Spectrosc Radiat Transf. 48 (1992) 9–24, https://doi.org/10.1016/0022-4073(92)90003-M.
[35] M.L. da Silva, M. Dudeck, Arrays of radiative transition probabilities for CO_2–N_2 plasmas, J Quant Spectrosc Radiat Transf. 102 (2006) 348–386, https://doi.org/10.1016/j.jqsrt.2006.02.018.
[36] M. Yousefi, P.F. Bernath, Line Lists for AlF and AlCl in the $X^1\Sigma^+$ Ground State, Astrophys. J. Suppl. Ser. 237 (2018) 8, https://doi.org/10.3847/1538-4365/aacc6a.
[37] A.G. Császár, G. Czakó, T. Furtenbacher, E. Mátyus, An active database approach to complete rotational–vibrational spectra of small molecules, Annual Reports in Computational Chemistry. 3 (2007) 155–176, https://doi.org/10.1016/S1574-1400(07)03009-5.
[38] T. Furtenbacher, A.G. Császár, J. Tennyson, MARVEL: measured active rotational–vibrational energy levels, J. Mol. Spectrosc. 245 (2007) 115–125, https://doi.org/10.1016/j.jms.2007.07.005.
[39] T. Furtenbacher, A.G. Csaszar, MARVEL: measured active rotational–vibrational energy levels. II. Algorithmic improvements, J. Quant. Spectrosc. Radiat. Transf. 113 (2012) 929–935, https://doi.org/10.1016/j.jqsrt.2012.01.005.
[40] R. Tóbiás, T. Furtenbacher, J. Tennyson, A.G. Császár, Accurate empirical rovibrational energies and transitions of $H_2{}^{16}O$, Phys. Chem. Chem. Phys. 21 (2019) 3473–3495, https://doi.org/10.1039/C8CP05169K.
[41] S.N. Yurchenko, A. Blissett, U. Asari, M. Vasilios, C. Hill, J. Tennyson, ExoMol molecular line lists – XIII. The spectrum of CaO, Mon. Not. Roy. Astron. Soc. 456 (2016) 4524–4532, https://doi.org/10.1093/mnras/stv2858.
[42] H.Y. Li, J. Tennyson, S.N. Yurchenko, ExoMol line lists – XXXII. The rovibronic spectrum of MgO, Mon. Not. Roy. Astron. Soc. 486 (2019) 2351–2365, https://doi.org/10.1093/mnras/stz912.
[43] Z. Qin, T. Bai, L. Liu, Line lists for the $X^2\Sigma^+$-$X^2\Sigma^+$, $A^2\Pi$-$A^2\Pi$ and $A^2\Pi$-$X^2\Sigma^+$ transitions of CP, J. Quant. Spectrosc. Radiat. Transf. 258 (2021), 107352, https://doi.org/10.1016/j.jqsrt.2020.107352.
[44] J. Tennyson, S.N. Yurchenko, The ExoMol project: Software for computing large molecular line lists, Int. J. Quantum Chem. 117 (2017) 92–103, https://doi.org/10.1002/qua.25190.
[45] M.B. Moeller, S.J. Silvers, Fluorescence spectra of PN and BF☆, Chem Phys Lett. 19 (1973) 78–81, https://doi.org/10.1016/0009-2614(73)87067-8.
[46] S.N. Yurchenko, A.F. Al-Refaie, J. Tennyson, ExoCross: a general program for generating spectra from molecular line lists, Astron Astrophys. 614 (2018) A131, https://doi.org/10.1051/0004-6361/201732531.
[47] P.S. Barklem, R. Collet, Partition functions and equilibrium constants for diatomic molecules and atoms of astrophysical interest, Astron Astrophys. 588 (2016) A96, https://doi.org/10.1051/0004-6361/201526961.
[48] A.W. Irwin, Polynomial partition function approximations of 344 atomic and molecular species, Astrophys. J. Suppl. Ser. 45 (1981) 621–633, https://doi.org/10.1086/190730.
[49] I. Jiménez-Serra, S. Viti, D. Quénard, J. Holdship, The Chemistry of Phosphorus-bearing Molecules under Energetic Phenomena, Astrophys J. 862 (2018) 128, https://doi.org/10.3847/1538-4357/aacdf2.
[50] J.C. Zapata Trujillo, A.-M. Syme, K.N. Rowell, B.P. Burns, E.S. Clark, M.N. Gorman, L.S. Jacob, P. Kapodistrias, et al., Computational Infrared Spectroscopy of 958 Phosphorus-Bearing Molecules, Front. Astronomy Space Sci. 8 (2021) 43, https://doi.org/10.3389/fspas.2021.639068.